Published in "Optics Communications 253: 4-6: 362-374, 2005"
which should be cited to refer to this work.

Powerful fast triggerable 6 μm laser for the muonic hydrogen 2S-Lamb shift experiment

A. Antognini [a,g,*], F.D. Amaro [b], F. Biraben [c], J.M.R. Cardoso [b], C.A.N. Conde [b], D.S. Covita [b], A. Dax [d,1], S. Dhawan [d], L.M.P. Fernandes [b], T.W. Hänsch [a], V.W. Hughes [d,✠], O. Huot [e], P. Indelicato [c], L. Julien [c], P.E. Knowles [e], F. Kottmann [f], Y.-W. Liu [h], J.A.M. Lopes [b], L. Ludhova [e,g], C.M.B. Monteiro [b], F. Mulhauser [e,2], F. Nez [c], B.N. Perry [j,3], R. Pohl [a,g], P. Rabinowitz [i], J.M.F. dos Santos [b], L.A. Schaller [e], C. Schwob [c], D. Taqqu [g], J.F.C.A. Veloso [b]

[a] *Max-Planck Institut für Quantenoptik, D-85748 Garching, Germany*
[b] *Departamento de Física, Universidade de Coimbra, PT-3000, Coimbra, Portugal*
[c] *Laboratoire Kastler Brossel, ENS, UPMC and CNRS, F-75252 Paris, CEDEX 05, France*
[d] *Physics Department, Yale University, New Haven, CT 06520-8121, USA*
[e] *Département de Physique, Université de Fribourg, CH-1700 Fribourg, Switzerland*
[f] *Labor für Hochenergiephysik, ETH-Hönggerberg, CH-8093 Zürich, Switzerland*
[g] *Paul Scherrer Institut, CH-5232 Villigen PSI, Switzerland*
[h] *Physics Department, National Tsing Hua University, Hsinchu 300, Taiwan*
[i] *Chemistry Department, Princeton University, Princeton, NJ 08544-1009, USA*
[j] *Exxon Research and Eng. Co., 1545 Rte 22, Annandale, NJ 08801, USA*

Received 4 November 2004; received in revised form 27 April 2005; accepted 27 April 2005

Abstract

Laser spectroscopy of the 2S-Lamb shift in muonic hydrogen (μ^-p) is being performed at the Paul Scherrer Institute, Switzerland, to determine the root-mean-square (rms) proton charge radius with 10^{-3} precision. A multistage laser system has been developed which provides 0.2 mJ pulse energy tunable at 6 μm wavelength. An excimer pumped dye laser

* Corresponding author. Tel.: +41 56 310 4614; fax: +41 56 310 5230.
E-mail address: aldo.antognini@psi.ch (A. Antognini).
[1] Present address: CERN, CH-1211 Geneva 23, Switzerland.
[2] Present address: University of Illinois at Urbana-Champaign, IL 61801, USA.
[3] Present address: 7 Barley Sheaf Road, Flemington, NJ, USA.
✠ Deceased.

is used to drive a titanium sapphire (Ti:Sa) system whose wavelength is then shifted to 6 μm using a multipass Raman cell filled with hydrogen. The short cavity length of the Ti:Sa oscillator (7 cm) guarantees a pulse width of 7 ns and a pulse energy of 1.2 mJ at 708 nm, a wavelength controlled by a mono-mode cw-Ti:Sa laser. The laser is triggered at a maximum 60 s^{-1} repetition rate by muons entering the apparatus at random times. A new type of multipass cavity has been developed to provide a homogeneously illuminated volume ($25 \times 7 \times 170$ mm^3).

PACS: 36.10.Dr; 42.60.By; 42.60.Da; 42.62.Fi; 42.65.Dr

Keywords: rms proton charge radius; Muonic hydrogen; Lamb shift; High energy 6 μm laser; Raman shift in hydrogen; Multipass 6 μm cavity; Frequency chirp

1. Introduction

The root-mean-square (rms) charge radius of the proton R_p is presently extracted either from electron–proton scattering or from hydrogen spectroscopy experiments. A recent reevaluation of all available electron–proton scattering data yields a value of $R_p = 0.895(18)$ fm [1]. Several atomic transition frequencies in hydrogen and deuterium have been measured and compared with calculations. The rms radius extracted from those spectroscopic data in the CODATA least square adjustment is $R_p = 0.8736(77)$ [2]. Another determination of the rms radius with 10^{-3} relative accuracy is possible by measuring the 2S-Lamb shift ΔE_{2P-2S} in muonic hydrogen ($\mu^- p$) [3–6]

$$\Delta E_{2P-2S} = 209.974(6) - 5.226 \cdot R_p^2 + 0.036 \cdot R_p^3 \text{ [meV]}, \quad (1)$$

where R_p is expressed in fm. In terms of frequency (1 meV $\approx$ 241.799 GHz) this energy splitting is about 50 THz, i.e., a wavelength of about 6 μm. The relative contribution of the proton size to ΔE_{2P-2S} is as much as 2%, two orders of magnitude more than for normal hydrogen. Therefore already a moderate accuracy in the measurement of ΔE_{2P-2S} leads to a significantly improved value of R_p.

We are pursuing an experiment at the Paul Scherrer Institute (PSI, Switzerland) to determine the 2S-Lamb shift in muonic hydrogen [7]. The goal is to measure the energy difference $\Delta E(2^5P_{3/2}–2^3S_{1/2})$ by laser spectroscopy to a precision of 30 ppm ($\sim$10% of the 18 GHz natural linewidth which is given by the 2P lifetime $\tau_{2P} \approx 10^{-11}$ s) and to deduce R_p with 10^{-3} relative accuracy.

The R_p value extracted by μp spectroscopy can be used to predict the 1S-Lamb shift in hydrogen [8]. A comparison of the predicted with the measured [9] 1S-Lamb shift leads to a bound-state QED test, whereas a subtraction of the predicted 1S-Lamb shift from the measured 1S–2S transition frequency in hydrogen leads to a better determination of the Rydberg constant (R_∞).

If R_p will become known with 10^{-3} relative accuracy from μp spectroscopy, bound-state QED calculations in hydrogen can be tested with a relative accuracy of 2×10^{-6}. A value of 3×10^{-7} may be reached in future when increased accuracy of other transition frequencies in hydrogen (e.g., 1S–3S) reduce the Rydberg constant uncertainty by a factor of 10. In contrast, the rms radius extracted from μp spectroscopy can be combined with the measured 1S–2S transition frequency in hydrogen [10] to reduce by a factor of 6 the uncertainty of R_∞ [11] if bound-state QED calculations are assumed to be correct.

In this paper, we report on a laser system that fulfills the requirements of this experiment. An overview of the experiment is given in Section 2 with focus on the features which constrain our laser system. The following sections contain detailed descriptions of the various components of the laser system: excimer–dye laser in Section 3, Ti:Sa laser and its frequency chirping in Section 4, the Raman shifter in Section 5, and the wavelength calibration of the whole system in Section 6. In Section 7, the 6 μm multipass cavity for the intensity enhancement is presented.

2. Experimental setup

The principle and the details of this experiment are given in [12,13]. The muonic hydrogen 2S-Lamb shift experiment uses a low density (0.6 mbar at room temperature) hydrogen target in which an ultra low energy μ^- beam is stopped, whereby highly excited μp atoms are formed [7]. Most of them deexcite quickly to the ground state, but ~1% form μp atoms in the 2S state which have a lifetime $\tau_{2S} = 1.3(2)$ μs [14]. A laser pulse tuned to ΔE_{2P-2S} irradiates the volume where the μp atoms are formed, about 1 μs after the muon stop. On resonance, excitation to the short lived 2P state occurs. The 1.9 keV X-ray emitted in the 2P–1S decay is detected in coincidence with the laser pulse [15]. A few laser-induced events per hour are expected on resonance which is sufficient to measure the 2S–2P resonance to the proposed accuracy [13].

Each arriving muon, before entering the hydrogen target, triggers the pulsed laser and the data acquisition system with a rate of about 240 s^{-1}. Muons are stopped in a volume of $17 \times 7 \times 170$ mm^3 which is then illuminated by the laser light.

The requirements on the laser system are summarized in Table 1. The most stringent requirement is a short delay between laser trigger and output 6 μm pulse. The laser has to be triggerable upon muon entry to the apparatus (rate of 240 s^{-1}) in a stochastic way, with a short delay <1.5 μs (due to the 1.3 μs lifetime of the 2S state at 0.6 mbar pressure), and has to have the shortest achievable dead time between two shots. A determination of the 2S–2P line position with 30 ppm precision corresponds to an accuracy of 1.5 GHz. The laser bandwidth has to be small compared with the natural linewidth of 18 GHz. The required tunability of the laser is determined by the uncertainty of the rms proton charge radius. For instance, the 2P–2S transition frequencies deduced from Eq. (1) for rms radius values of 0.895 and 0.8736 fm are, respectively, 49765.5 and 49812.9 GHz (i.e., 1660.00 and 1661.58 cm^{-1}). Consequently, the search range of the laser has to be of the order of 250 GHz to take into account the rms proton radius uncertainty.

Table 1
Requirements on the laser system for the muonic hydrogen 2S–2P Lamb shift measurement

Requirements		Comments
Frequency	50 THz	Corresponding to $\lambda = 6$ μm
Bandwidth	<2 GHz	$\Gamma_{2S-2P} = 18$ GHz (FWHM)
Tunability	250 GHz	Large R_p uncertainty
Energy/pulse	$\gtrsim 0.2$ mJ	Illuminated vol. $25 \times 7 \times 170$ mm^3
Triggerability	Stochastic	μ^-p formation time is random
Repetition rate	100 s^{-1}	100 s^{-1} results in 1 event/hour
Delay	<1.5 μs	1.3 μs lifetime of the 2S state
Reliability	10^8 shots	Many days with 100 s^{-1} shots

Muonic hydrogen has a reduced mass 186 times that of normal hydrogen causing oscillator strengths $1/(186)^3$ times weaker than the corresponding ones in hydrogen. The energy density required to saturate the 2S–2P transition is 16.5 mJ/cm^2. This density has to be obtained in the atom–laser interaction volume of $17 \times 7 \times 170$ mm^3. This is achieved if the 6 μm laser system provides pulses with ~0.2 mJ energy. Reliability of the whole system during the measuring time of about 200 h during the beam time period of few weeks is essential.

For reasons we will discuss below we developed a laser system whose main components are shown in Fig. 1. Two high power XeCl excimer lasers provide the pumping energy (320 mJ each) for the whole system. Their pulses have a 1.2 μs delay relative to the trigger signal. No other laser with such a short delay and large pulse energy is commercially available. Each excimer pumps a two-stage multimode nontunable dye laser which convert the 308 nm excimer laser pulses to 45 mJ pulses at 540 nm. They in turn pump an injection-seeded oscillator–amplifier titanium sapphire (Ti:Sa) laser system which delivers 12 mJ at 708 nm. The wavelength tunability and bandwidth of the Ti:Sa oscillator, and therefore of the subsequent amplifier and 6 μm light, is controlled by a single-mode cw-Ti:Sa laser stabilized on a calibrated Fabry–Perot (FP) cavity.

Wavelength conversion from the visible to the infrared is made by a third-Stokes Raman shifter operated with 14 bar H_2 gas. For our conditions, efficient Raman conversion needs the TEM_{00} mode and pulse lengths less than 10 ns in duration, which is obtainable with a short cavity length

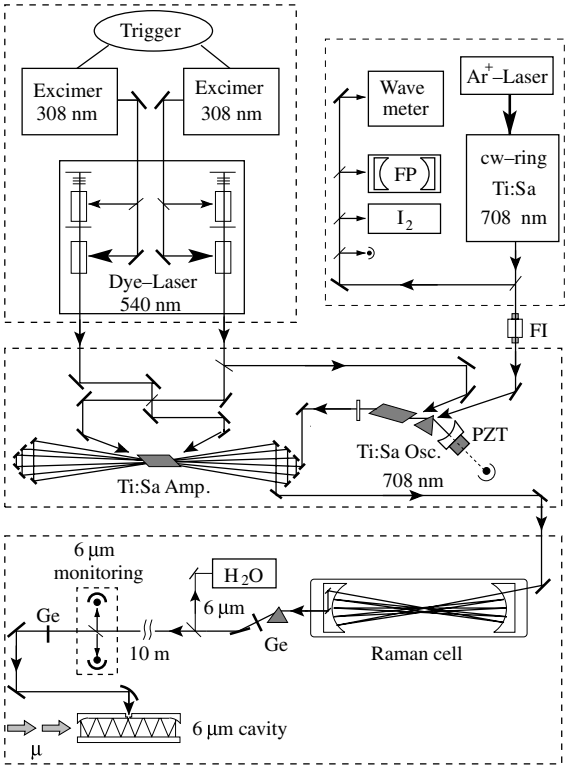

Fig. 1. Schematic view of the laser system. The main components are a pulsed excimer–dye laser system, a tunable cw-Ti:Sa laser, a pulsed oscillator–amplifier Ti:Sa laser, a Raman cell, and a 6 μm multipass mirror cavity with its diagnostic system. FP: Fabry–Perot, I_2: iodine absorption cell, H_2O: water absorption cell, PZT: piezo transducer, FI: Faraday isolator.

Ti:Sa oscillator. The third-Stokes Raman shifter converts the wavelength from 708 nm to the 6 μm region yielding a pulse energy of 0.2 mJ.

The infrared light is transported over a 12 m long path to the mirror cavity surrounding the muon stop volume. Two mirrors located on the left and right side of the muon stop volume form a nonresonant 6 μm multipass cavity. One of the mirrors has a hole of 0.6 mm diameter where the laser light is focused and enters the cavity. The light then is reflected back and forth between the two mirrors and spread out almost homogeneously illuminating the whole μ^- stopping volume. The part of the confined light which is reflected back at the hole position escapes from the multipass cavity and is detected by a fast infrared photo-detector. This provides a diagnostic for the light circulation inside the multipass cavity.

This laser scheme was developed since in the 6 μm region, there exist no commercially available tunable and rapidly triggerable lasers which provide sufficient energy. However, a tunable 6 μm laser can be realized by using a tunable laser in the visible region (e.g., Ti:Sa) pumped by a high power laser. Its wavelength can then be converted (frequency mixing, OPO, Raman) to 6 μm. Stochastic triggering and short delay excludes the use of a standard high-power low-repetition-rate (<100 Hz) Nd:YAG laser as they require around 100 ms for inversion build-up. Continuously pumped Q-switched YAG lasers can possibly provide the necessary pulses but available commercial models have too low pulse energy and too long delay times (2 μs) due to the use of AOM switching and low gain per pass. Hence we decided to use excimer lasers which can be triggered within 1 μs and provide sufficient energy to fulfill our requirements. For efficient down-conversion to the 6 μm wavelength, we used a H_2 Raman cell with low threshold and high efficiency. Possible alternative schemes could be constructed using an OPO-based $HgGaS_2$ crystal [16] or by frequency mixing methods [17] but the reliability at relatively high repetition rates has not yet been demonstrated.

3. Excimer–dye lasers

3.1. Excimer lasers

The most restrictive requirement on the laser system is the short delay between muon arrival and laser pulse. Two commercial Lambda Physik series LPX 200 XeCl excimer lasers are used each of which delivers 320 mJ output energy and has a maximal repetition rate of 100 Hz. The trigger electronics of the excimer lasers was modified to decrease the internal delay to 1.2 μs.

The time necessary to recharge the laser capacitor bulk is 10 ms, and during this dead time the laser is inoperable. When the laser is stochastically triggered the dead time has to be enlarged to 12.5 ms to avoid intolerable energy and profile fluctuations of the dye laser output pulse. A muon trigger

rate of 240 s^{-1} and a laser dead time of 12.5 ms results in an average laser repetition rate of 60 $s^{-1} \approx (1/240 + 0.0125)^{-1}$ s^{-1}. This means that the laser is fired on average for every fifth detected muon which enters the target.

3.2. Dye lasers

Each of the two excimer lasers pumps its own dye laser oscillator–amplifier system. The oscillator is free running with a 10 cm long linear flat–flat resonator. Each resonator has a $T =$ 10% output-coupler, an 8-element-Brewster-plate polarizer, and a Bethune dye cell. The Bethune (prism) cell allows homogeneous transverse pumping, yielding a nearly Gaussian transverse profile [18]. The oscillator resonator length is made as short as possible to maximize the time overlap between the oscillator pulse and the excimer pulse within the dye amplifier cell. The dye laser oscillators are pumped with 12% of the available excimer laser light and deliver 20 ns long pulses (see Fig. 3) with 5 mJ at 540 nm. These pulses are then amplified to 45 mJ, leading to an optical-to-optical efficiency of 14%. Pulse to pulse energy fluctuations are of about 10% and strongly depend on the time between successive pulses (those typical values are measured with new dye solutions and at a stochastic rate of 60 s^{-1}). In contrast to the oscillator, the amplifier cells are not Bethune cells, but are transversely pumped from one side only, which results in a nonuniform illumination over the cross section of the excited volume. The highest gain which occurs right on the inner face of the cuvette side wall causes diffraction effects. A reduction of those effects and an enhancement of the dye lifetime is accomplished by reducing the solvent viscosity, increasing the dye solution flow, and decreasing the dye concentration. For the same reason, the output energy and profile quality progressively decreases with increasing repetition rate.

Several dyes were tested that have an emission band that overlaps with the absorption band of Ti:sapphire [19,20]: Coumarin 102, pure and mixed with DABCO (a triplet quencher), pure Coumarin 307, Coumarin 153 mixed with DABCO, and Rhodamine 6G, pure and mixed with DABCO. We found that the combination of Coumarin 153 with DABCO has the longest lifetime under the intense UV irradiation of our XeCl excimer lasers, and it was therefore used.

Propylene-carbonate, methanol, and ethanol were tested as dye solvents. Methanol and ethanol show similar behavior and, when compared with propylene-carbonate, give a factor of three longer dye lifetime and 20% more output energy at 50 Hz. A further factor of two enhancement of the dye lifetime is achieved by dissolving the triplet quencher DABCO in the dye solution. The dye-lasers with 5.5 l dye solution each (Coumarin 153 + DABCO + methanol) showed an energy output decrease of 13% in 4 h when operated at 50 Hz. Methanol is used in the amplifier cells, whereas the oscillators are operated with the more expensive ethanol solvent because methanol produces the formation of a white coating on the Bethune cell tube wall. This layer, which dramatically reduces the energy output, is strongly dependent on the surface quality of the tube walls, and does not occur with ethanol. Methanol is employed in the amplifier cells which have better surface quality and do not exhibit this effect. The dye mixture of the oscillator consists of 0.8 g Coumarin 153 and 2.0 g DABCO per liter of ethanol, whereas the amplifier mixture consists of 1.0 g dye with 2.0 g DABCO per liter of methanol.

During data taking the dye solutions were changed in average 2–3 times a day, that is about 30 l of dye solution are used per day (15 h of operation). As said above the typical efficiency with new dye is about 14% whereas the dye was exchanged when its efficiency was around 12%.

The gas mixtures of the excimer lasers are exchanged once per day, and the excimer laser optics are cleaned at the same time.

4. Ti:Sa oscillator and amplifier

4.1. Oscillator

The resonator arrangement of the pulsed Ti:Sa oscillator is presented in Fig. 2. The design

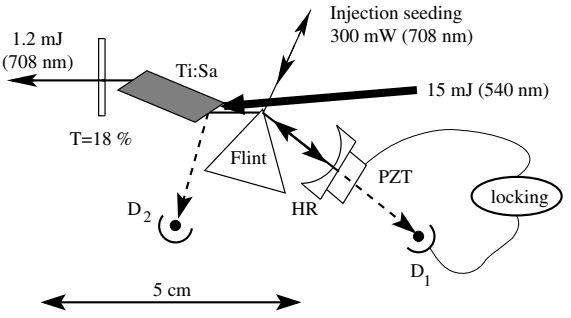

Fig. 2. Ti:Sa oscillator resonator. High reflector: HR, Piezoelectric element: PZT, photodiodes D_1 and D_2.

maximizes the output pulse energy, minimizing the output pulse duration. The short optical resonator length of 7 cm results in a short output delay (56 ns) relative to the pump pulse, and creates a short pulse length (7 ns). The Brewster-cut Ti:Sa crystal (15 mm path length, $\alpha = 1.8\ \mathrm{cm}^{-1}$, with a figure of merit >300 [21]) is placed in a flat–concave (4 m radius of curvature) stable resonator. At 708 nm, the gain in the crystal is half that of the maximum [20], so that an equilateral flint prism, inserted at minimum deviation angle, is needed to force the oscillation at 708 nm. The oscillator frequency is precisely controlled by injection seeding from a cw-ring Ti:Sa laser [22].

At a stochastic rate of 60 s^{-1}, the Ti:Sa oscillator delivers 1.2 mJ per pulse at 708 nm when pumped with 15 mJ from one dye laser. Between 10 and 60 s^{-1} a 20% decrease in pulse energy at 708 nm is observed that can be attributed to a deterioration of the dye laser beam quality. The beam energy and profile of the 540 nm pump laser deteriorates as the delay time between pulses shortens.

4.2. Injection seeding

Injection seeding is chosen for wavelength selection and tuning of the pulsed oscillator. The simplicity and precision of the cw-laser frequency control is directly transferred to the pulsed oscillator. Beside the prism no other wavelength selective elements are needed in the oscillator which minimizes optical losses within the resonator, maximizing the output energy.

A Ti:Sa cw-laser in a ring geometry, pumped by an Ar^+ laser, is used as the seed source [22]. The 1.6 m long cavity is equipped with three wavelength selective elements controlled by feedback loops: a Lyot filter, a thin etalon, and an internal FP. A 1 MHz bandwidth is obtained by servo-locking the cavity length with a piezo-mounted mirror to a stable external FP cavity. An output power of 400 mW at 708 nm is achieved with 5 W pumping power. The frequency stability of the cw-Ti:Sa laser is given by the external FP cavity (see Section 6).

The 708 nm cw-light is resonantly coupled into the oscillator cavity via reflection on the prism surface (see Fig. 2). Light incident on the prism at the minimum deviation angle $\alpha_{\min} = 53.72°$ ($\alpha_{\mathrm{Brewster}} = 58.19°$) is partially reflected toward the high reflector (HR). The low coupling efficiency (0.23%) requires a large cw power of 300 mW, but has the advantage that there is only weak optical feedback (cw and pulsed) to the cw-cavity. Because of its unidirectional ring cavity geometry, the cw-Ti:Sa laser is highly insensitive to any feedback, but a Conoptic 713 Faraday isolator (see Fig. 1) is used to further reduce feedback, mainly because of the wavemeter.

The cavity length of the pulsed 708 nm oscillator is servo-locked to the cw-laser frequency. Proper operation of the injection seeding is monitored by observing the temporal profile of the pulse on the fast photodiode D_2 and monitoring the oscillator pulse wavelength with a spectrometer. When the oscillator is injection seeded, the pulse build-up time is typically shortened from 95 to 55 ns.

4.3. Chirp in the Ti:Sa oscillator

As will be further discussed in Section 6 the calibration of the whole laser system is performed directly at 6 μm. However this occurs only few times during data taking. In between, the frequency of our laser source is controlled by the cw-Ti:Sa laser at 708 nm with the help of a calibrated FP. A variation of the frequency shifts caused by a variation of the chirping effect will thus lead to a small error in the determination of the output frequency at 6 μm. The chirp occurring in the Ti:Sa oscillator are studied in order to determine the size of this frequency shift variation.

Ideally, the oscillator frequency should be equal to that of the seed cw laser and its bandwidth given by the Fourier transform of its pulse length. However some frequency shift and additional broadening occur due to time dependent changes in the Ti:Sa crystal refractive index caused by optical and thermal effects during the pulsed pumping and the lasing process [23]. Therefore we developed a simple model to describe the frequency changes during the pulse formation.

When a laser beam traveling in z-direction in a medium extending from z_0 to z_1 experiences a time-dependent refractive index n, its instantaneous frequency ν at z ($z_0 < z < z_1$) is given by [24]

$$\nu(z,t) = \nu(z_0,t_0) - \frac{1}{\lambda}(z-z_0)\frac{\mathrm{d}n}{\mathrm{d}t}, \tag{2}$$

where λ is the wavelength inside the medium. The frequency shift $\Delta\nu$ experienced by a wave traveling inside the oscillator cavity is given by Eq. (2) [24]:

$$\Delta\nu = -\frac{L_\mathrm{c}}{\lambda}\frac{\Delta n}{\Delta t}, \tag{3}$$

where Δn is the refraction index change in Δt and L_c the crystal length.

There are two sources of change of refractive index: one related to the excited population density N^exc and the other one related to the crystal temperature T which vary during the pulse formation. The pumping and lasing processes dynamically affect the inversion population, inducing a change of the refractive index which is [25].[4]

$$\Delta n^\mathrm{opt} = C^\mathrm{opt}\, N^\mathrm{exc} \quad \text{with}$$
$$C^\mathrm{opt} = (1.4 \pm 0.6) \times 10^{-24}\ \mathrm{cm}^3. \tag{4}$$

This has to be attributed to the susceptibility difference between the excited and ground state of the Ti^{3+} ions. In addition, there is an increase of the crystal temperature ΔT during pumping (phonon relaxation between excited states) and lasing (phonon relaxation to the ground state). The resulting T-induced change in refractive index can be calculated using $\Delta n^\mathrm{therm} = (\mathrm{d}n/\mathrm{d}T)\Delta T$ with $\mathrm{d}n/\mathrm{d}T = 12.6 \times 10^{-6}\ \mathrm{K}^{-1}$ [21].

The elementary rate equations for the number of photons $m(t)$ inside the cavity and the inverted population $N^\mathrm{exc}(t)$ are used to model the pulse formation in the oscillator cavity [26]:

$$\frac{\mathrm{d}m(t)}{\mathrm{d}t} + \gamma_\mathrm{c} m(t) = +KN^\mathrm{exc}(t)m(t), \tag{5}$$
$$\frac{\mathrm{d}N^\mathrm{exc}(t)}{\mathrm{d}t} + \gamma_2 N^\mathrm{exc}(t) = -KN^\mathrm{exc}(t)m(t) + P_\mathrm{p}(t), \tag{6}$$

where γ_c is the total cavity decay rate, γ_2 and P_p the decay and pumping rate of the inverted population and K is the coupling coefficient between photons and atoms describing the stimulated emission.

Numerical integration of Eqs. (5) and (6) permits tracing the pulse formation $m(t)$ and the evolution of the population inversion $N^\mathrm{exc}(t)$ during the pulse buildup. The pump intensity time profile and the pump-to-output pulse delay are taken from measurements. Only the absolute value of the pump energy density is assumed to be a free parameter since the pump beam size at the crystal surface is poorly known. It is tuned to have a pump-to-output pulse delay equal to the experimentally determined one (see Fig. (3)).

Pulse length and energy of the oscillator pulse $m(t)$ resulting from the model reasonably reproduce the measured values. Moreover $N^\mathrm{exc}(t)$ and $\mathrm{d}N^\mathrm{exc}(t)/\mathrm{d}t$ combined with Eq. (4) and the $\mathrm{d}n/\mathrm{d}T$ value, predict the time evolution of the refractive index. The frequency shift is then determined using Eq. (3) and is plotted in Fig. 3. The frequency changes from a value of about -170 MHz (relative to the cw) at the pulse leading edge to -85 MHz at the pulse tail (see Fig. 3). A mean chirp shift with respect to the cw-seeder of $\Delta\nu = -(110 \pm 30)$ MHz and a broadening of $\delta\nu_\mathrm{chirp} = (65 \pm 30)$ MHz (FWHM) are therefore expected. The uncertainty is dominated by the error in C^opt.

The frequency shift between the cw-injected light and the pulsed output light is measured by scanning the I_2 absorption line labeled "430" in [27]. Both pulsed and cw-laser light are injected into a 50 cm long cell operated at a I_2 gas pressure

[4] The C value given in [25] takes into account not only the purely optical change of refraction index, but also the thermal contribution by lasing. Associated with each *photon* emitted from the excited state there is a relaxation *phonon* in the ground state. From Fig. 2 of the cited article, the thermal component can be extracted and subtracted from the value $C = (1.1 \pm 0.5) \times 10^{-24}\ \mathrm{cm}^3$ to give the purely optical component $C^\mathrm{opt} = (1.4 \pm 0.6) \times 10^{-24}\,\mathrm{cm}^3$.

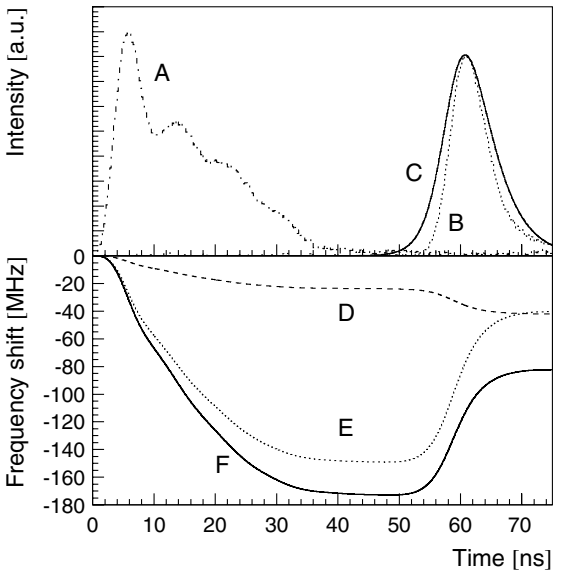

Fig. 3. Time distributions of measured and simulated pulse intensities and frequency shift for the Ti:Sa oscillator. (Top): Measured pump pulse intensity (A), measured output pulse intensity (B), and simulated output pulse intensity (C). (Bottom): Simulated oscillator frequency shift versus time caused by the thermal effect (D), optical effect (E), and the sum (F).

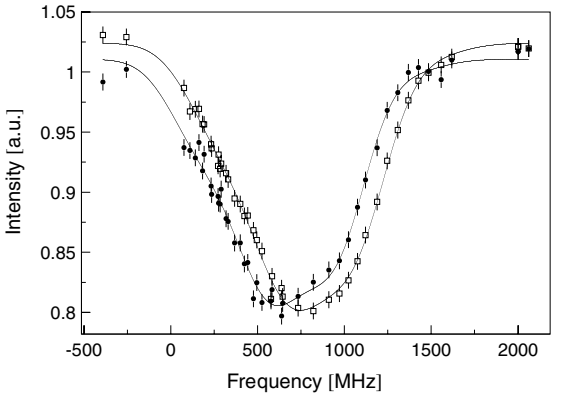

Fig. 4. Frequency scan of the cw-Ti:Sa master laser (full circles) and pulsed oscillator slave laser (empty squares) over an iodine absorption line. In both cases the detuning of the master laser relative to a FP fringe defines the frequency axis.

of 2 mbar, and a temperature of 365 °C. Their transmission curves are shown in Fig. 4. The asymmetric line shape is caused by the underlying unresolved components of the transition. The transmitted cw light is fit using a phenomenological model with seven Gaussian functions, which defines the reference absorption line shape. The absorption measurement of the pulsed light is fit with the reference line shape convoluted with an additional Gaussian which describes the pulsed laser spectral distribution. The position of the additional Gaussian gives the mean frequency shift whereas its width gives the laser bandwidth. A simultaneous fit of both absorption measurements is performed ($\chi^2 = 83$ for 80 degrees of freedom). The laser shift and width uncertainty extracted from the fit procedure are conservatively enlarged by a factor of 2 to take into account possible inaccuracies of the line-shape model. A (-110 ± 10) MHz red shift of the pulsed light relative to the seed laser frequency is measured, in good agreement with the above chirp model. A laser width of (130 ± 120) MHz (FWHM) is measured which is in agreement with the theoretically estimated width (Fourier-limit $\sim$125 MHz (FWHM), frequency chirp $\sim$65 MHz).

The chirping might cause lasing at a second longitudinal mode. A scan over a frequency range of ± 3 GHz has hence been performed but no evidence for a second longitudinal mode is noticeable.

The simple model developed above to estimate the frequency shift predicts a dependence of the frequency shift on the pump pulse energy (see Fig. 6 in [23]). The pulse-to-pulse dye energy fluctuations and slow variations (due to dye and excimer gas degradation) cause frequency shift variations of about 20 MHz.

4.4. Ti:Sa amplifier

The oscillator output pulse (1.2 mJ at 708 nm) is amplified roughly by a factor of 10 in an eight-pass amplifier (see Fig. 1). The beam is refocused on each pass. The amplifier crystal is pumped longitudinally from both sides, and water cooled to 10 °C. The maximum optical-to-optical energy conversion efficiency was 18%, but the routine operating conditions are normally 14%.

The amplification process is more efficient for the leading edge of the pulse and thus a pulse shortening is expected. A reduction of pulse width from 7 to 6 ns (FWHM) between input and output

pulse is measured. Similar to the oscillator, the amplifier introduces some frequency chirp. The resulting frequency shift per pass $\Delta\nu^{\text{pass}}$ is

$$\Delta\nu^{\text{pass}} = -\frac{L_c C}{\lambda}\frac{\Delta N^{\text{exc}}}{\Delta t'}, \tag{7}$$

where ΔN^{exc} is the change of inversion population in the time $\Delta t'$ necessary to cross the crystal. The experimental relation $\Delta n = CN^{\text{exc}}$ with $C = (1.1 \pm 0.5) \times 10^{-24}$ cm^3 is used [25].[5] The pumping process does not induce any frequency shift because the crystal is pumped before the red pulse from the oscillator reaches it. Only the change of population inversion caused by the red pulse amplification leads to a frequency shift. The chirp resulting from the eight-pass amplifier is estimated to be (20 ± 15) MHz, which is negligible in the context of our experiment.

5. Raman cell

Sequential vibrational Raman scattering in H_2 in a multiple-pass-cell [28] of the Herriott-type [29] is used to convert the 708 nm pulse to the 6 μm region. Hydrogen is ideally suited for this purpose since it not only provides reasonable gain at modest pump intensities, but also has the largest Stokes shift ($Q_{01}(1) = 4155.2$ cm^{-1}). Three sequential Raman shifts convert an input wavenumber of 14128 cm^{-1} (corresponding to 708 nm) by 3×4155.2 cm^{-1}, to 1662 cm^{-1} (which is 6.02 μm) passing through 1.00 μm (first Stokes) and 1.72 μm (second Stokes). Any tuning of the input wavenumber tunes the output wavenumber by the same amount.

The Raman cell, a 2 m long steel tube, is filled with 14 bar of H_2 (<1 ppm impurities). It encloses two spherical silver-coated copper mirrors (1 m radius of curvature, 12.7 cm diameter, with dielectric protection layer [30]) and a measured reflectivity of $R = 97.7\%$ at 708 nm. The two mirrors form a stable spherical interferometer. The mirror spacing is 1.9325 m giving a confocal parameter $b = 36.1$ cm and a 33 passes configuration with Herriott's parameters $\mu = 14$, $\nu = 17$ [31]. Both mirrors have a 1.27 cm diameter off-axis hole for injection and extraction of the light beam. Pulse extraction occurs before ray path closure. Light at 708 nm is mode matched to the confocal parameter with a Galilean telescope.

This configuration provides optimal enhancement of the conversion at each pass. The gain coefficient (exponent) per pass, g, for Stokes beams with the same confocal parameter b, is given in MKS units by [28]

$$g = \frac{16\pi P \chi_r''}{(1+\lambda_p/\lambda_s)\lambda_s^2 n_s n_p \epsilon_0 c}\tan^{-1}\left(\frac{L}{b}\right), \tag{8}$$

where λ_p and λ_s are the pump and Stokes wavelengths, P the pump power, L the length of the gain medium, χ_r'' the Raman susceptibility, n_p and n_s the indices of refraction at pump and Stokes frequencies, c the speed of light, and ϵ_0 the free space permittivity. For a mirror reflectivity R, the net gain exponent g_n after n transits through the cell, assuming the same reflection loss for Stokes and pump beams at each reflection, is given by [32]

$$g_n = g\frac{1-R^n}{1-R}. \tag{9}$$

For a pulse at 708 nm with 12 mJ energy and of 6 ns length, Eq. (8) indicates that the gain from noise will produce the first Stokes in the first half pass, and the second Stokes within the second pass. For the third Stokes production with $g = 0.4$, the remaining 31 passes are essential. However, using Eq. (9) with a reflectivity $R = 97.7\%$ and $n = 31$ a total gain exponent of only $g_n = 9$ is achieved. The obtained output energy at 6 μm can therefore be explained only if four-wave mixing which initializes the third Stokes radiation is taken into consideration [33,34].

Because of water absorption in the second and third Stokes region, the cell is equipped with a gas circulating system connected to a cold trap which removes water from the amplifying medium. Pump photons (708 nm), first Stokes (1.00 μm), second Stokes (1.72 μm), first rovibrational Stokes (1.07 μm), second rovibrational Stokes (1.91 μm) and weaker first (547 nm) and second (446 nm) anti-Stokes together with the 6.02 μm third Stokes photons exit the Raman cell. A CaF_2 prism is used

[5] In contrast to the oscillator case, the constant C of [25] can be inserted directly here.

to separate the 6 μm light, and two AR-coated (5–8 μm) Ge-plates remove all parasitic light remaining on the 6 μm beam axis.

Fig. 5 shows the 6 μm output of the Raman cell plotted as a function of the 708 nm input pulse energy. A threshold pump energy of 6.5 mJ is visible. With an average input energy of 12 mJ, a mean output energy of 0.2 mJ at 6 μm is measured which corresponds to a quantum efficiency of 14%. An input pulse length of 6 ns, the shortest pulse length delivered by the Ti:Sa laser, is chosen to maximize the Raman efficiency. In the steady state regime the Raman gain scales with the pump power (see Eq. (8)), favoring short pulses, whereas the gain decreases for very short pulses when the transient regime becomes dominant [35].

6. Frequency calibration of the 6 μm light

Calibration of the 6 μm pulse wavelength is performed by measuring a water absorption line. The line at 6.014 μm (1662.80968(7) cm^{-1}) labeled "37" in Ref. [36] is scanned by tuning the cw-laser at 708 nm. The cw-laser is referenced to a calibrated FP cavity with a free spectral range of 1.5 GHz [37]. The FP cavity is made of mirrors optically contacted on a Zerodur spacer and maintained under vacuum (7×10^{-6} mbar) by an ion pump. The vacuum cell is inserted in a heavy brass box to attenuate mechanical vibration and fast thermal fluctuation. Its resulting long term stability is measured to be better than 10 MHz over several weeks [38]. A wavemeter is used to unambiguously determine the FP fringe number.

The absorption measurements were made by having the 6 μm light traverse a 37 cm long cell filled with 55 mbar of air at 35% humidity ($T = 23$ °C). Additional desorption from the walls results in a H_2O partial pressure of 1.0(5) mbar. Similar measurements are performed at 20 and 3 mbar total pressure. The 6 μm beam line is flushed with dry N_2 gas to avoid absorption by water vapor in the ambient air. Averaging over 128 pulses per point is necessary because of the intensity fluctuations of the 6 μm laser. Fig. 6 shows the transmitted 6 μm laser beam intensity versus the cw-Ti:Sa laser frequency referenced relative to one FP fringe. The errors are estimated based on the scatter of multiple measurements at a subset of frequency points.

The absorption curve is fit with the function

$$F^{\text{laser}}(\nu) \otimes (1 - \exp\{-L^{\text{pressure}}(\nu) \otimes G^{\text{Doppler}}(\nu)\}), \tag{10}$$

where $\otimes$ represent the convolution operator, and F^{laser} is the laser spectral distribution with amplitude, position and width as free parameters. L^{pressure} describes the pressure broadening (Lorentzian with $\Gamma = 325$ MHz [39]), and G^{Doppler}

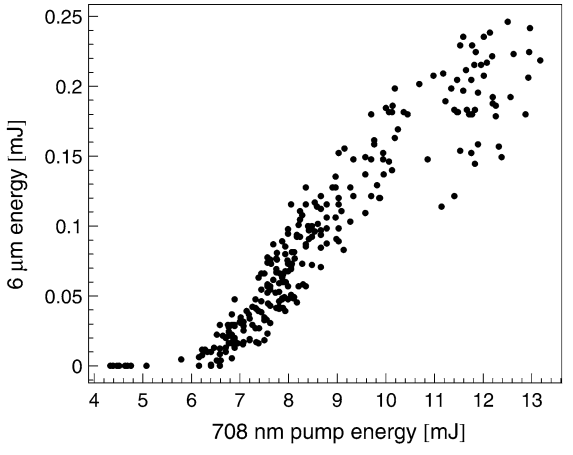

Fig. 5. Measurements of the Raman conversion efficiency. Plotted is the third Stokes (6 μm) output energy versus the 708 nm pump pulse energy.

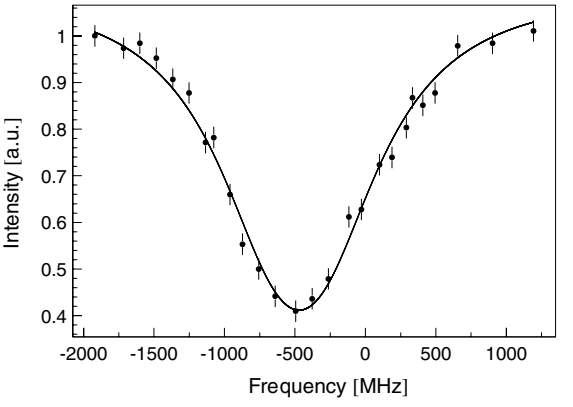

Fig. 6. Wavelength calibration of the 6 μm light by scanning a water line. The intensity transmitted through a 37 cm long cell filled with 55 mbar air is plotted versus frequency relative to a Fabry–Perot fringe at 708 nm.

the Doppler broadening (Gaussian with 150 MHz at FWHM) of the water line. The statistical error in the determination of the line-center position is 10 MHz. This error was enlarged to 50 MHz to accommodate for systematics caused by possible laser frequency drift since the laser is not locked to the FP during the scan. The gain narrowing process in the Raman cell may cause F^{laser} to be different from a Lorentzian corresponding to a pressure broadened Raman transition. The absorption measurement is fit for the two extreme cases of a purely Lorentzian and a purely Gaussian laser spectral distribution. The resulting laser bandwidths are (540 ± 30) and (820 ± 40) MHz, respectively. We assumed an average value of (680 ± 140) MHz at FWHM.

At the water line position the 6 μm wavelength can thus be calibrated regardless of possible systematic shifts in the various stages from the 708 nm cw-light to the 6 μm region.

Dye laser energy variations cause frequency shift variations in the pulsed Ti:Sa laser of about 20 MHz, a broadening which has to be quadratically added to the 50 MHz fit uncertainty. For the 2S-Lamb shift measurement the resonance is scanned by locking the cw-laser on various FP fringes. The laser has to be tuned by less than 100 FP fringes from the water calibration line to cover the whole anticipated 2S–2P resonance region. The FP free spectral range is known with an accuracy of about 1 kHz at 708 nm, therefore, the uncertainty of the 6 μm wavelength over the whole scanning region is 55 MHz (quadratic sum of 50, 20, and 100×0.001 MHz).

The absolute FP calibration is performed at the Ti:Sa wavelength. The FP is calibrated at 778–794 nm with three Rb lines known to a precision <1 MHz [38] and at 700–708 nm with six I_2 lines known to a precision of 200 MHz [27]. The positions of the measured FP transmission peaks ν_i referenced to the atomic lines are fit using the following equation [37]:

$$\nu_i - \nu_r = I_0(N_i - N_r)(1 - \epsilon(N_i + N_r)), \qquad (11)$$

where ν_r corresponds to the FP peak close to the 778 nm Rb line (chosen as reference frequency), I_0 is the zero order free spectral range, $N_i \sim 3 \times 10^5$ the fringe number, and $\epsilon \sim 10^{-10}$ a phenomenological parameter which takes into account frequency dependent mirror spacing corrections. The FP parameters ϵ and I_0 are extracted from the fit and used to determine the frequency of any FP transmission peak around 708 nm with an absolute precision better than 200 MHz.

A comparison between the water line position at 6 μm and the corresponding cw-laser frequency measured with the FP at 708 nm gives a value of 4155.219(1) cm^{-1} for the $Q_{01}(1)$ Stokes shift in H_2 at 295 K and 14.0(1) bar. This is in acceptable agreement with values given in [40]. Corrections for the chirps of (-110 ± 10) MHz measured in the Ti:Sa oscillator, and of (20 ± 15) MHz calculated for the amplifier are taken into account.

The 6 μm light bandwidth of (680 ± 140) MHz measured at the Raman cell exit is much broader than the 708 nm bandwidth of the Ti:Sa pulse which is measured to be (130 ± 120) MHz (cf. Section 4.3). It can be concluded that the Raman gain process contributes a broadening of about 650 MHz.

This number can be compared to the upper limit of the broadening given by the spectral width of the Raman gain, which at our conditions is 690 MHz (see Eq. (1) in Ref. [40]). The maximum expected broadening for the three sequential Stokes shifts is therefore about 2 GHz. This value is reduced to the measured 650 MHz by gain narrowing processes occurring during the Stokes pulse build up.

7. The 6 μm multipass cavity

The 6 μm light is coupled into an intensity enhancement cavity, placed inside the hydrogen target for the excitation of the 2S–2P transition. Fig. 7 shows the geometry of the mirror multipass cavity. The μ^- stopping volume, $17 \times 7 \times 170$ mm^3, is elongated in direction of the muon beam (z-axis) because of the low H_2 pressure. The laser light illuminates the stop volume transversely, because it is not possible to mount laser mirrors on the muon beam axis. Therefore rather long laser mirrors left and right of the muon beam are used. Above and below the muon beam, the X-ray detectors have to be positioned as close as possible to the muon beam for solid angle efficiency. Hence the vertical

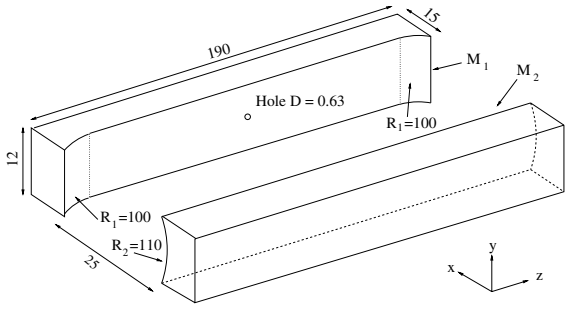

Fig. 7. Sketch of the 6 μm multipass cavity. The figure is distorted to visualize details. All dimensions are given in mm.

dimension of the laser mirrors is made as small as possible. Twelve millimeter high mirrors turned out to be large enough to illuminate a 7 mm high volume. Laser light enters the cavity through a 0.63 mm diameter hole in one mirror (see Fig. 7) and is reflected between the two mirrors illuminating a volume of $25 \times 7 \times 170$ mm^3. By observing the intensity of the part of the 6 μm light which escapes of the multipass cavity, we obtain an average lifetime of about 140 ns. Taking into account the distance between the cavity mirrors (25 mm), that corresponds to 1700 reflections between the two mirrors. This lifetime is determined not only by the mirror reflectivity and spacing but also by the unavoidable escape of light out of the injection hole. In fact, confined light which is reflected back at the hole position will escape the cavity, and this escaping light is used to monitor the cavity alignment.

Since the time integrated spatial intensity distribution of the light inside the cavity is relatively homogeneous, the fluence F is given approximately by

$$F \approx \frac{E_{\text{in}}^{\text{laser}} n_{\text{refl}}}{A_{\text{cav}}}, \tag{12}$$

where $E_{\text{in}}^{\text{laser}}$ is the pulse energy entering the cavity, $n_{\text{refl}} = 1700$ the measured average number of reflections, and $A_{\text{cav}} = 17 \times 0.7$ cm^2 the illuminated transverse cavity area. A 6 μm laser pulse energy of 0.12 mJ is therefore sufficient to saturate the 2S–2P transition (corresponding to a fluence of $F \approx 16.5$ mJ/cm^2). A μp(2S) atom which has survived to the time the laser enters the cavity has thus a probability of $(1 - e^{-1})$ to be excited to the 2P-state if the laser is resonant with the transition and is providing a pulse with 0.12 mJ energy. Including various losses on the beam path from the Raman cell to the 6 μm cavity, about 0.2 mJ are required at the Raman cell exit to saturate the transition.

8. Conclusion

We have developed a powerful, fast triggerable, high quality 6 μm laser beam with 60 s^{-1} (stochastic) repetition rate. Two excimer pumped dye lasers operating at 540 nm are used to pump an oscillator–amplifier Ti:Sa laser. A reliable and simple injection seeded Ti:Sa oscillator has been developed. An output pulse of 1.2 mJ energy, 7 ns width at 708 nm is achieved (without the use of Q-switching methods), with a pump energy of 15 mJ. The simulated oscillator characteristics (pulse length, energy output and frequency chirp) are in good agreement with the measured values. The eight-pass Ti:Sa amplifier delivers a pulse energy of 12 mJ at 708 nm which is converted to 6 μm via a Raman shifter. The Raman cell produces 0.2 mJ of 6 μm light corresponding to a quantum efficiency of 14%.

The total delay of the 6 μm pulse from trigger to multipass cavity entry is 1.6 μs, corresponding to the sum of the following delays: excimer–dye laser (1220 ns), Ti:Sa oscillator (56 ns), Ti:Sa amplifier (45 ns), Raman cell (200 ns) and various beam paths (80 ns). The laser tunability is between 5.5 to 7 μm. The maximal wavelength is limited by the Raman gain which decreases at longer wavelength (see Eq. (8)) whereas the minimal wavelength is limited by the spectral profile of the Ti:Sa gain. The absolute frequency of the tunable 6 μm source stabilized on an external FP is deduced from a water line absorption measurement with an accuracy of 55 MHz; the bandwidth is 680 MHz.

To enhance the intensity of the 6 μm light, a multipass cavity providing a large illuminated volume ($25 \times 7 \times 170$ mm^3) has been developed.

The 6 μm source, the multipass cavity and associated diagnostics meet all the requirements for the muonic 2S-Lamb shift experiment and have been

operated continuously for 4 weeks during the search for the 2S–2P resonance. Steps of 10.5 GHz (corresponding to 7 FP fringes) were used to search for the 2S–2P resonance. The laser was shot for 15 different frequencies, distributed around the frequency given by Eq. (1) inserting the CODATA 1998 [41] value for the proton rms radius. The laser was shot for each FP value for about 7 h. The scanned range was limited by the time available at the accelerator. The data are presently being analyzed.

Acknowledgments

This work was performed at the Paul Scherrer Institute, Switzerland. We acknowledge support from the Swiss National Science Foundation, the Swiss Academy of Engineering Sciences, the BQR de l'UFR de physique fondamentale et appliquée de l'Université Paris 6, the program PAI Germaine de Staël no. 07819NH du ministère des affaires étrangères France, the Foundation for Science and Technology (FCT) Lisbon, the FEDER through the Project POCTI/FNU/41720/2001, and the US Department of Energy.

The authors thank: B. Leoni and Z. Hochman for technical support; T. Gerber with his Reaction Analysis Group, and R. Bombach for providing us laser components and helpful advice; H.-J. Kluge and W. Nörthershäuser of GSI Darmstadt for providing us dye pumps, excimer and Ar^+ lasers; R. Zenobi and A. Renn of the Department of Chemistry at ETH Zurich for a dye pump and an Ar^+ laser; and H. van Den Bergh of EPFL Lausanne for an excimer laser.

The principle design of the laser system was proposed by H.P. von Arb. We thank also the PSI accelerator division, workshop, Hallendienst, and other support groups for their valuable help.

References

[1] I. Sick, Phys. Lett. B 576 (2003) 62.
[2] P. Mohr, B. Taylor, Rev. Mod. Phys. 77 (2005) 1.
[3] M. Eides, H. Grotch, V. Shelyuto, Phys. Rep. 342 (2001) 63.
[4] K. Pachucki, Phys. Rev. A 53 (1996) 2092.
[5] K. Pachucki, Phys. Rev. A 60 (1999) 3593.
[6] P. Indelicato et al., in: P. Kienle et al. (Eds.), International Workshop of Exotic Atoms, Austrian Academy of Sciences Press, Vienna, 2003, p. 61.
[7] F. Kottmann et al., Hyperf. Int. 138 (2001) 55.
[8] K. Pachucki, U. Jentschura, Phys. Rev. Lett. 91 (2003) 113005.
[9] B. de Beauvoir et al., Eur. Phys. J. D 12 (2000) 61.
[10] M. Niering et al., Phys. Rev. Lett. 84 (2000) 5496.
[11] P. Mohr, Private communication.
[12] R. Pohl et al., Can. J. Phys. 83 (2005) 339.
[13] F. Kottmann et al., in: P. Kienle et al. (Eds.), International Workshop of Exotic Atoms, Austrian Academy of Sciences Press, Vienna, 2003, p. 159.
[14] R. Pohl, Ph.D. Thesis, Swiss Federal Institute of Technology (ETHZ), Switzerland, 2001. Available from http://e-collection.ethzbib.ethz.ch/index.html.
[15] L. Ludhova et al., Nucl. Instrum. Methods A 540 (2005) 169.
[16] K.L. Vodopyanov et al., Appl. Phys. Lett. 75 (1999) 1204.
[17] K. Kato, IEEE J. Quantum Electron. 20 (1984) 698.
[18] D.J. Brink, C.J. van der Hoeven, Rev. Sci. Instrum. 55 (1984) 1948.
[19] Radiant Dyes Laser Accessories, D-42929 Wermelskirchen, Germany.
[20] P.F. Moulton, J. Opt. Soc. Am. B 3 (1986) 125.
[21] The Roditi International Corp., London, England W1B 5SE.
[22] S. Bourzeix et al., Opt. Commun. 99 (1993) 89.
[23] P. Bakule, Appl. Phys. B 71 (2000) 11.
[24] N. Melikechi, S. Gangopadhyay, E.E. Eyler, J. Opt. Soc. Am. B. 11 (1994) 2402.
[25] K.F. Wall et al., Opt. Lett. 14 (1989) 180.
[26] A.E. Siegman, Lasers, University Science Books, Sausalito, CA, 1986 (Chapter 24).
[27] S. Gerstenkorn, P. Luc, Atlas du spectre d'absorption de la molecule de l'iode entre 14000–15600 cm^{-1}, Ed. CNRS II, 91405 Orsay, France.
[28] P. Rabinowitz, B. Perry, N. Levinos, IEEE J. Quantum Electron. QE-22 (1986) 797.
[29] D. Herriott, H. Kogelnik, R. Kompfner, Appl. Opt. 3 (1964) 523.
[30] SPAWR Optical Research Inc., Lake Havasu City, AZ 86403, USA.
[31] B.N. Perry et al., Opt. Lett. 5 (1980) 288.
[32] P. Rabinowitz et al., Appl. Phys. Lett. 35 (1979) 739.
[33] W.R. Trutna, R.L. Byer, Appl. Opt. 19 (1980) 301.
[34] B.N. Perry et al., Opt. Lett. 10 (1985) 146.
[35] R.L. Carman et al., Phys. Rev. A 2 (1970) 60.
[36] R. Poth, J. Mol. Spectrosc. 190 (1998) 379.
[37] R. Battesti et al., Phys. Rev. Lett. 92 (2004) 253001.
[38] R. Battesti, Ph.D. Thesis, Université P. et M. Curie. Available from: <http://tel.ccsd.cnrs.fr/>, 2003.
[39] L.S. Rothman, J. Quant. Spectrosc. Radiat. Transfer 82 (2003) 5.
[40] W.K. Bischel, M.J. Dyer, Phys. Rev. A 33 (1986) 3113.
[41] P. Mohr, B. Taylor, Rev. Mod. Phys. 72 (2000) 351.